

ChemComm

Chemical Communications

Accepted Manuscript

This article can be cited before page numbers have been issued, to do this please use: Y. Li, L. Sutrisno, Y. Hou, Y. Fei, C. Xue, Y. Hu, M. Li and Z. Luo, *Chem. Commun.*, 2020, DOI: 10.1039/D0CC03667F.



This is an Accepted Manuscript, which has been through the Royal Society of Chemistry peer review process and has been accepted for publication.

Accepted Manuscripts are published online shortly after acceptance, before technical editing, formatting and proof reading. Using this free service, authors can make their results available to the community, in citable form, before we publish the edited article. We will replace this Accepted Manuscript with the edited and formatted Advance Article as soon as it is available.

You can find more information about Accepted Manuscripts in the [Information for Authors](#).

Please note that technical editing may introduce minor changes to the text and/or graphics, which may alter content. The journal's standard [Terms & Conditions](#) and the [Ethical guidelines](#) still apply. In no event shall the Royal Society of Chemistry be held responsible for any errors or omissions in this Accepted Manuscript or any consequences arising from the use of any information it contains.

COMMUNICATION

A redox-activatable biopolymer-based micelle for the sequentially enhanced mitochondria-targeted photodynamic therapy and hypoxia-dependent chemotherapyReceived 00th January 20xx,
Accepted 00th January 20xx

DOI: 10.1039/x0xx00000x

Yanan Li^{†a}, Linawati Sutrisno^{†b}, Yanhua Hou^c, Yang Fei^a, Chengcheng Xue^a, Yan Hu^b, Menghuan Li^{*a}, Zhong Luo^{*a}

A tumor redox-activatable micellar nanoplatfom based on the natural-occurring biomacromolecule hyaluronic acid (HA) was developed for the complementary photodynamic/chemotherapy against CD44-positive tumors. Here HA was first conjugated with L-carnitine (Lc)-modified zinc phthalocyanine (ZnPc) via disulfide linkage and then co-assembled with tirapazamine (TPZ) to afford the physiologically-stable micellular nanostructure. The mitochondrial-targeted photodynamic activity of ZnPc-Lc could efficiently activate the mitochondrial apoptosis cascade and deplete the oxygen in the tumor intracellular environment to amplify the hypoxia-dependent cytotoxic effect of TPZ.

Recently, there's an upsurge in developing antitumor nanotherapeutics with natural-occurring biopolymers such as proteins, peptides and polysaccharides, which may offer unique properties over their synthetic counterparts including high biocompatibility, biodegradability and low immunogenicity.^{1, 2} Hyaluronic acid (HA) is a promising candidate of those biopolymers and holds potential for clinical translation.^{3, 4} Specifically, HA is a hydrophilic linear macromolecular polysaccharide composed of glucuronic acid and N-acetylglucosamine. It's one of the major components in the extracellular matrix (ECM) of both healthy and malignant tissues and has intrinsic biocompatibility and biodegradability. Remarkably, HA molecules contain many hydroxyl, carboxyl and N-acetyl groups for the facile coupling of various therapeutic substances. Meanwhile, HA could provide long circulation time and enhanced safety due to its high hydrophilicity and low immunogenicity. More importantly, HA could bind to the CD44 glycoproteins overexpressed on many types of tumor cells, leading to improved therapeutic index and lower systemic toxicity.^{5, 6} These properties make HA particularly relevant for tumor-targeted drug delivery.

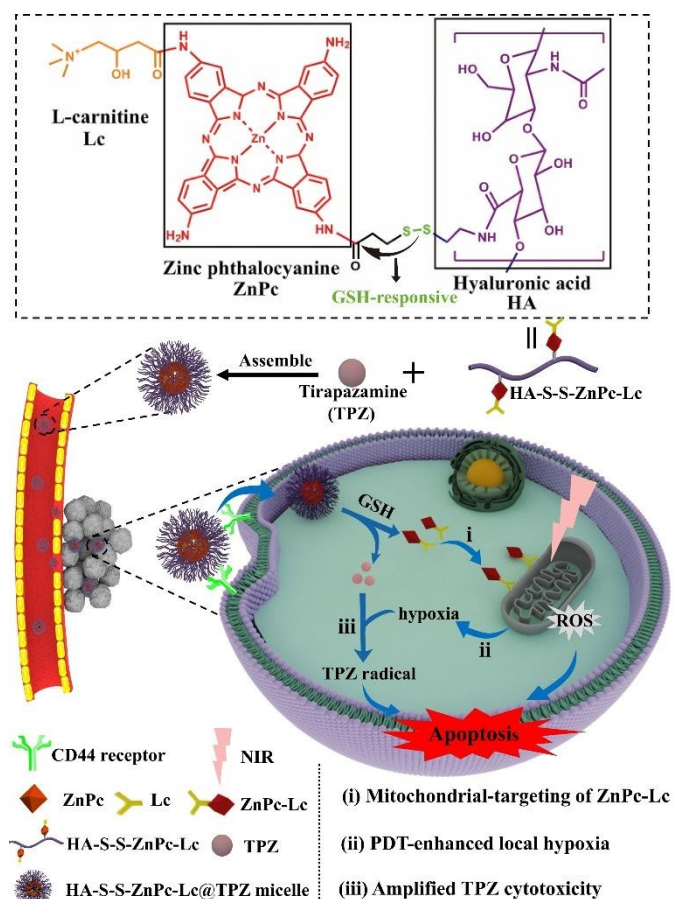
In addition to biopolymer-based drug delivery technologies, scientists are also searching for new therapeutic agents and

strategies for tumor treatment to improve the tumor treatment outcome. Typically, tirapazamine (TPZ) is an emerging bioreductive prodrug that could be converted into cytotoxic radicals in hypoxic tumor intracellular environment,^{7, 8} which is a universal feature for many tumor indications.^{9, 10} TPZ is a benzotriazine compound that could be metabolized by both one- and two-electron reductases in tumor cells under hypoxic conditions and form highly reactive radicals, which would then react with tumor DNA to cause single-strand breaks, double-strand breaks and chromosome aberrations, leading to potent tumor inhibition effect.¹¹ Nevertheless, the efficacy of TPZ may be compromised by the spatial heterogeneity of oxygen availability in tumor tissues.¹² To overcome these obstacles, TPZ is usually combined with photodynamic therapy (PDT), which could consume the intracellular oxygen to produce cytotoxic reactive oxygen species (ROS).¹³ However, the biological half-life of ROS is usually very low, which may attenuate the antitumor activity of PDT in vivo.¹⁴ Therefore, new modification and release mechanisms are urgently needed to coordinate the therapeutic activity of PDT and TPZ to enhance the eventual treatment outcome.

Here, we report a redox-activatable micellar nanoplatfom based on HA to deliver L-carnitine (Lc)-modified zinc phthalocyanine (ZnPc) and TPZ to CD44-positive tumor cells for complementary mitochondria-targeted PDT and TPZ treatment (Scheme 1).¹⁵ Specifically, the ZnPc-Lc photosensitizers were first conjugated onto the HA backbone via disulfide bond and then self-assembled with TPZ molecules to afford the physiologically stable micelles, which demonstrated long blood circulation time and were effectively taken in by CD44-positive tumor cells via HA-CD44 interaction. The disulfide bond could then be cleaved by the excess glutathione (GSH) in tumor intracellular environment and detach the ZnPc-Lc, which would destabilize the micelles and release the TPZ. Due to the high positive charge and lipophilicity of ZnPc-Lc, it would home to the negatively-charged mitochondrial membrane and initiate the mitochondrial apoptosis cascade via the in-situ NIR-activated PDT. Meanwhile, the mitochondria-targeted PDT would also consume the oxygen in the tumor cytosol and facilitate the activation of TPZ in a synergistic manner. It's anticipated that

^a School of Life Science, Chongqing University, Chongqing 400044, China^b Key Laboratory of Biorheological Science and Technology, Ministry of Education, College of Bioengineering, Chongqing University, Chongqing 400044, China^c Chongqing Engineering Research Center of Pharmaceutical Sciences, Chongqing Medical and Pharmaceutical College, Chongqing 401331, P. R. China.[†] These authors contributed equally to this paper.

Electronic Supplementary Information (ESI) available: [details of any supplementary information available should be included here]. See DOI: 10.1039/x0xx00000x



this study may offer new avenues to suppress tumor proliferation with reduced adverse effects.

We first immobilized ZnPc onto the HA backbone via thiol-disulfide exchange (Figure S1), during which ZnPc reacted with 3-(2-pyridyldithio) propanoic acid via carbodiimide reaction and was then grafted to the thiolated HA at a loading ratio of around 8% (wt/wt) (Figure S3). Lc moieties were then conjugated to ZnPc via carbodiimide reaction and confirmed using ^1H NMR spectra, UV-vis spectroscopy and zeta potential (Figure S2 and Figure S3). HA-S-S-ZnPc-Lc would then co-assemble with TPZ via an oil-in-water emulsion approach to form micelles (Figure S1) with a TPZ loading ratio of around 4% (Figure S3). The micelles have a spherical shape with distinct boundaries (Figure 1e), and their average diameter is around 200 nm (Figure 1c), which is optimal for passive targeting. Zeta potential analysis indicated that the surface charge of the HA biopolymer has increased slightly after the ZnPc conjugation from -28.0 mV to -20.0 mV due to the amine groups in ZnPc and the surface charge of HA-S-S-ZnPc-Lc (-16.0 mV) was even higher than HA-S-S-ZnPc due to the highly positively charged Lc groups (Figure S3). Meanwhile, UV-vis absorption results showed that a new peak emerged at around 270 nm for HA-S-S-ZnPc-Lc@TPZ micelles compared to pristine HA-S-S-ZnPc-Lc, suggesting successful TPZ incorporation (Figure 1a). The HA-S-S-ZnPc-Lc has a CMC (critical micelle concentration) of 0.045 mg/mL (Figure 1b),

suggesting the high stability of the micelles in body fluids and beneficial to enhance the tumor specific accumulation.

The redox-sensitivity of the micelle under GSH stimulation was then investigated via UV-vis spectroscopy. As shown in Figure 1d, minimal TPZ leakage (nearly 10%) was observed in the control group within 50 hours, suggesting the excellent stability of the micelles. In contrast, the final TPZ release ratio reached 70% under 10 mM of GSH. It was also observed that the amount of the TPZ release was positively correlated with the incubation time, indicating that GSH could be exploited as a redox trigger to regulate the release patterns of TPZ. We also monitored the morphological changes of the micelles before and after the GSH treatment via TEM and found that the micelles have been disintegrated into small fragments after incubation in the GSH-containing solution for 24 h (Figure 1e), further validating with the proposed drug release mechanism based on the GSH-triggered micelle destabilization. Considering the high level of GSH inside tumor cells, this feature is beneficial for preventing the undesirable activation of the drug-loaded micelles in healthy cells and tissues.¹⁶

We then monitored the targeting effect of the micelles by comparing their uptake by CD44-positive 4T1 cells and CD44-negative HUVECs (healthy primary endothelial cells). FITC was used to label the ZnPc moieties to indicate their cellular distribution patterns. Only negligible FITC fluorescence was found in HUVECs incubated with micelles for 2 h (Figure 2a and

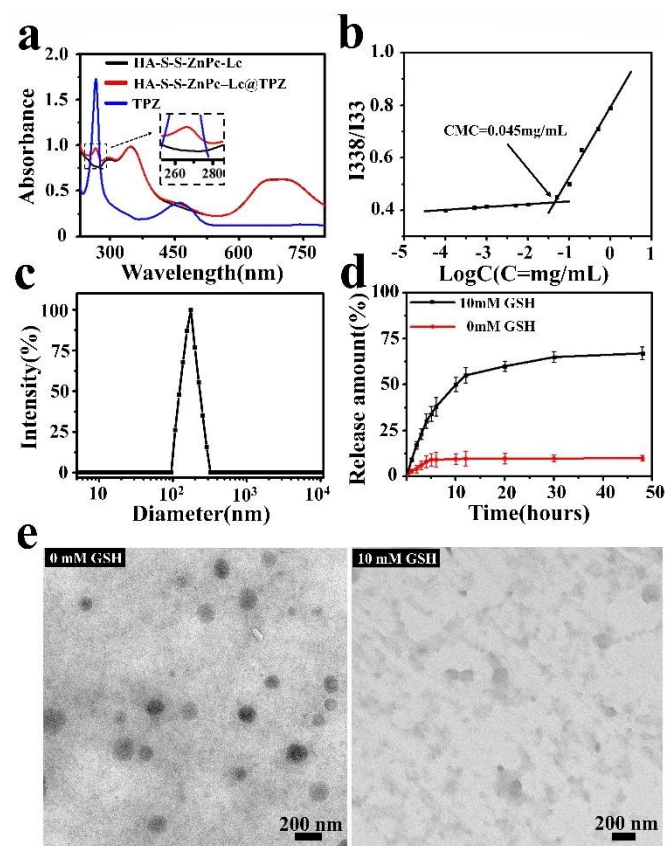


Figure 1. (a) The UV-vis absorption spectra of the HA-S-S-ZnPc-Lc and HA-S-S-ZnPc-Lc@TPZ. Inserted image shows the enhanced absorption around 270 nm due to TPZ incorporation. (b) The critical micelle concentration of HA-S-S-ZnPc-Lc. (c) Size distribution of HA-S-S-ZnPc-Lc@TPZ micelles. (d) Release profile of TPZ after incubation with and without GSH ($n=6$). (e) Morphological changes of the HA-S-S-ZnPc-Lc@TPZ micelles after incubation with 10 mM GSH for 24 h.

Figure S4), while micelle-treated 4T1 cells showed evidently stronger FITC fluorescence. Meanwhile, the FITC fluorescence in the HA-pretreated 4T1 cells remained at a low level comparable to HUVECs due to the saturation of the membrane CD44. Statistical analysis further revealed that the total FITC fluorescence intensity in the biopolymer-treated 4T1 cells was more than two-fold higher than the CD44-negative HUVECs (Figure S5). These results implied that HA-S-S-ZnPc-Lc@TPZ micelles could be efficiently endocytosed by 4T1 tumor cells due to HA-CD44 interaction, thus potentiating tumor-specific drug deposition while sparing healthy cells. Furthermore, we extended the incubation time to 24 h and observed the cellular distribution patterns of the micelles after endocytic uptake. As depicted in Figure 2b and Figure S6, the red fluorescence (mitotracker) in the HA-S-S-ZnPc-Lc@TPZ group has almost overlapped with the green fluorescence (FITC-labeled ZnPc-Lc) with a colocalization ratio of 0.71, while those in the HA-S-S-ZnPc@TPZ group were still largely separated (colocalization ratio: 0.3), indicating that the Lc-modified ZnPc has been attached to the mitochondrial membrane.

Besides, we also explored the PDT-induced ROS generation and cellular deoxygenation. It was observed all groups showed negligible ROS generation without NIR and the oxygen levels remained normal, indicated by the minimal green and red fluorescence in the intracellular environment (Figure 2d and Figure S7). Contrastingly, high level of intracellular ROS has been observed in HA-S-S-ZnPc-Lc and HA-S-S-ZnPc-Lc@TPZ groups under NIR irradiation (720 nm, 200 mW/cm², 5 min), accompanied by increasing local hypoxia. The results support our hypothesis that the ZnPc-mediated PDT could generate large amount of cytotoxic ROS by consuming the cytosolic oxygen, thus creating synergies with the co-delivered TPZ. Subsequently, we monitored the photodynamic damage of the micelles on tumor mitochondria by investigating the changes in the mitochondrial transmembrane potential ($\Delta\Psi_m$) via JC-1 staining, during which the normal and damaged mitochondria were stained red or green, respectively. The HA-S-S-ZnPc-Lc+NIR group showed strong green fluorescence with almost no red fluorescence (Figure 2c and Figure S8), evidently suggesting the severe mitochondrial damage thereof. In comparison, the HA-S-S-ZnPc+NIR group only showed modest green fluorescence, which blended with the strong red fluorescence of undamaged mitochondria and led to a yellowish fluorescence pattern. The modest mitochondrial damage in the HA-S-S-ZnPc+NIR group could be explained by the dissipation of ROS by the reductive species in tumor cytosol. We also measured the cytosolic levels of cytochrome c (cyt c) using western blot assay and found that the intracellular cyt c levels in HA-S-S-ZnPc-Lc+NIR and HA-S-S-ZnPc-Lc@TPZ+NIR groups have increased by almost three-fold compared to the control group (Figure S10), indicating the severe mitochondrial damage thereof. These results again confirmed the mitochondria-targeting capability of the micelles as well as its augmenting effect on PDT efficacy.

We further investigated the antitumor efficacy of the micelles against CD44-positive tumors in vitro. Only slight growth inhibition has been observed in non-NIR groups due to the lack of effective treatment (Figure S9). Meanwhile, the

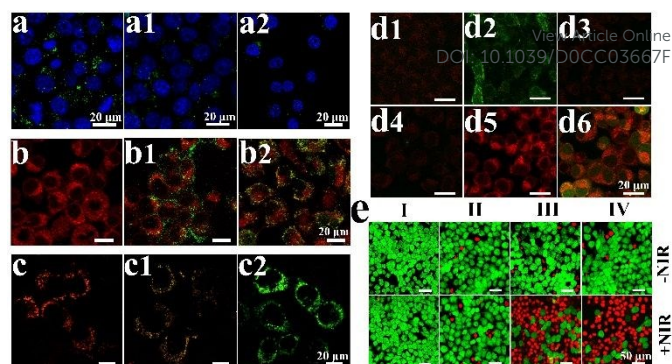


Figure 2. (a) CLSM images of 4T1 cells after incubation with HA-S-S-ZnPc-Lc-FITC. (a1) CLSM images of CD44-blocked 4T1 cells after incubation with HA-S-S-ZnPc-Lc-FITC. The cells were pretreated with HA (5 mg/mL) for competitive CD44 binding. (a2) CLSM images of HUVECs cells treated with HA-S-S-ZnPc-Lc-FITC. Scale bars: 20 μ m. (b) CLSM images showing tumor mitochondria (red fluorescence) and the intercellular distribution of FITC-labeled biopolymers (green fluorescence) after treatment with PBS (b), HA-S-S-ZnPc-FITC (b1) and HA-S-S-ZnPc-Lc-FITC (b2). CLSM images of 4T1 cells stained with JC-1 to assess the mitochondrial damage after treatment with PBS (c), HA-S-S-ZnPc+NIR (c1) and HA-S-S-ZnPc-Lc+NIR (c2). (d) CLSM images on the changes in the intracellular ROS and hypoxia levels in 4T1 cells after treatments with PBS (d1), ROS inducer (d2), HA-S-S-ZnPc-Lc (d3), PBS+NIR (d4), hypoxia inducer (d5), HA-S-S-ZnPc-Lc + NIR (d6). The ROS inducer and hypoxia inducer were added as positive control. (e) Live/dead cell imaging of 4T1 cells after treatment with (I) PBS, (II) TPZ, (III) HA-S-S-ZnPc-Lc and (IV) HA-S-S-ZnPc-Lc@TPZ micelles with or without laser irradiation.

survival rate of HA-S-S-ZnPc/HA-S-S-ZnPc-Lc-treated cells remained the same to the control group, indicating the excellent biocompatibility of the micelles. In comparison, the cell viability in the HA-S-S-ZnPc group dropped to 48.4% after NIR treatment, which was attributed to the ZnPc-mediated PDT. The survival rate was even lower in the HA-S-S-ZnPc-Lc+NIR group at 38.5%, which indicates that modifying ZnPc with Lc moieties could enhance the overall efficacy of PDT. The most pronounce tumor inhibition effect was observed in the HA-S-S-ZnPc@TPZ+NIR group, which clearly demonstrated the superior antitumor efficacy by combining mitochondria-targeted PDT and the hypoxia-augmented TPZ chemotherapy. Markedly, the tumor inhibition efficiency of HA-S-S-ZnPc@TPZ and HA-S-S-ZnPc-Lc@TPZ is statistically different at lower TPZ concentrations, but the difference became non-significant when the equivalent TPZ concentration reached 10 μ g/mL due to the diminished antitumor susceptibility at larger nanoformulation concentrations.¹⁷ The MTT results were also supported by the flow cytometry analysis and live/dead cell staining (Figure S11 and Figure 2e).

The antitumor efficacy of the micelles was evaluated on 4T1 tumor-bearing mice. It was demonstrated that more than 30% of the injected micelles accumulated in tumors (Figure 3a, Figure S13) thanks to the size-mediated passive targeting and HA-mediated active targeting. Meanwhile, no apparent drug deposition was detected in the central nervous system due to the protecting effect of the blood brain barrier therein (Figure S12). The micelles also showed prolonged blood retention capability and were almost eliminated from the body after 96 h of incubation (Figure S12), thus providing balanced treatment and safety performance. Next, we investigated the changes in tumor sizes to evaluate the treatment response. As shown in Figure 3b, tumors in the PBS and PBS+NIR groups grew rapidly due to the lack of effective treatment. Meanwhile, tumors in the TPZ+NIR group showed negligible growth inhibition due to the low cytotoxicity of TPZ under normoxic conditions. In comparison, significant tumor suppression was observed in the

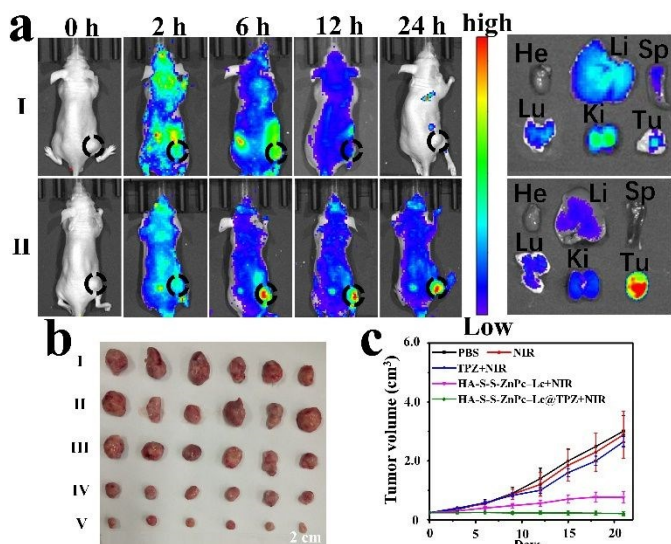


Figure 3. (a) Changes in the systemic distribution of (I) Cy5 and (II) Cy5-labeled micelles in tumor-bearing mice after tail vein injection. Black dash circles indicate the tumor region. Images on the right show the organ distribution of the Cy5-labeled micelles at 24 h post injection. (b) Visual comparison of the sizes of extracted tumor after 21-day treatment with PBS (I), PBS+NIR (II), TPZ+NIR (III), HA-S-S-ZnPc-Lc+NIR (IV) and HA-S-S-ZnPc-Lc@TPZ+NIR (V). (c) Quantitative analysis on tumor volumes throughout the 21-day treatment period.

HA-S-S-ZnPc-Lc+NIR group ($p < 0.01$) due to the combined PDT and hypoxia-enhanced TPZ chemotherapy, in which the final tumor volume decreased to 762 mm³ (Figure 3c). Remarkably, the final tumor volume in HA-S-S-ZnPc-Lc@TPZ+NIR group was the smallest at 210 mm³ ($p < 0.01$), suggesting that modifying ZnPc with Lc could reduce ROS dissipation in intracellular environment and enhance the potency of the PDT. The trends above were also consistent with the hematoxylin and eosin (H&E) and terminal deoxynucleotidyl transferase mediated dUTP nick end labeling (TUNEL) assay on tumor tissue samples (Figure S15), in which the HA-S-S-ZnPc-Lc@TPZ + NIR group demonstrated the highest apoptosis levels. In addition, no apparent changes have been observed in the mouse body weight and histological analysis of major organs in the biopolymer-treated groups, implying the high biocompatibility of the micelles (Figure S14 and Figure S16). The in vivo results demonstrated that the biopolymer-based micelles could effectively deliver ZnPc-Lc and TPZ into CD44-positive tumors in a highly targeted manner and efficiently eliminate the tumor cells through the combinational treatment of mitochondria-targeted PDT and hypoxia-enhanced TPZ chemotherapy at optimal safety.

Conclusions

In summary, we developed a redox-activatable micellar nanoplatform based on a natural polysaccharide hyaluronic acid for the tumor-targeted delivery of mitochondria-targeted photosensitizers (ZnPc-Lc) and tirapazamine (TPZ), leading to complementarily enhanced PDT and chemotherapy. The micelles could be disintegrated by the excess GSH in tumor cells and release ZnPc-Lc and TPZ into the tumor cytosol. The positively charged Lc moiety in the lipophilic ZnPc-Lc molecules would then guide them to the negatively charged mitochondria and damage the mitochondrial membrane via NIR-actuated ROS generation, which could not only enhance the cytotoxic effect of the short-lived ROS, but also consume the oxygen in the tumor cytosol to amplify the antitumor efficacy of TPZ. The high biocompatibility, delivery efficiency and sequentially

enhanced PDT/chemotherapy of the biopolymer-based micelle is favorable for the treatment against a variety of tumor indications, which may also facilitate the development of more advanced nanotherapeutics for combinational tumor therapy.

Conflicts of interest

There are no conflicts to declare.

Notes and references

† This work was financially supported by National Key R&D Program of China(2017YFB0702603, 2016YFC1100300), National Natural Science Foundation of China (11832008, 51773023), Fundamental Research Funds for the Central Universities (2020CDJQY-A075, 2020CDJYGL009), Returning Overseas Scholar Innovation Program (CX2018062), Chongqing Outstanding Young Talent Supporting Program(CQYC201905072) and Natural Science Foundation of Chongqing Municipal Government (cstc2018jcyjAX0368) and Chongqing Research Program of Basic Research and Frontier Technology (Grant No. cstc2018jcyjAX05 80).

- E. Rideau, R. Dimova, P. Schwillle, F. R. Wurm and K. Landfester, *Chem. Soc. Rev.*, 2018, **47**, 8572-8610.
- J. X. Ding, J. Zhang, J. N. Li, D. Li, C. S. Xiao, H. H. Xiao, H. H. Yang, X. L. Zhuang and X. S. Chen, *Prog. Polym. Sci.*, 2019, **90**, 1-34.
- F. Zamboni, S. Vieira, R. L. Reis, J. M. Oliveira and M. N. Collins, *Prog. Mater. Sci.*, 2018, **97**, 97-122.
- I. L. M. Isa, S. A. Abbah, M. Kilcoyne, D. Sakai, P. Dockery, D. P. Finn and A. Pandit, *Sci. Adv.*, 2018, **4**, eaaq0597.
- G. L. Huang and H. L. Huang, *J. Control. Release*, 2018, **278**, 122-126.
- Y. F. Tang, Y. Y. Li, X. M. Hu, H. Zhao, Y. Ji, L. Chen, W. B. Hu, W. S. Zhang, X. Li, X. M. Lu, W. Huang and Q. L. Fan, *Adv. Mater.*, 2018, **30**, 1801140.
- Y. Liu, Y. Jiang, M. Zhang, Z. Tang, M. He and W. Bu, *Acc. Chem. Res.*, 2018, **51**, 2502-2511.
- Y. Q. Ye, Q. S. Hu, H. Chen, K. Liang, Y. Yuan, Y. Xiang, H. Ruan, Z. Zhang, A. R. Song, H. W. Zhang, L. X. Liu, L. X. Diao, Y. Y. Lou, B. Y. Zhou, L. Wang, S. T. Zhou, J. J. Gao, E. Jonasch, S. H. Lin, Y. Xia, C. R. Lin, L. Q. Yang, G. B. Mills, H. Liang and L. Han, *Nat. Metab.*, 2019, **1**, 431-444.
- X. S. Li, N. Kwon, T. Guo, Z. Liu and J. Yoon, *Angew. Chem.-Int. Edit.*, 2018, **57**, 11522-11531.
- Z. Tang, Y. Liu, M. He and W. Bu, *Angew. Chem.-Int. Edit.*, 2019, **58**, 946-956.
- S. Yang, Z. Tang, C. Hu, D. Zhang, N. Shen, H. Yu and X. Chen, *Adv. Mater.*, 2019, **31**, 1805955.
- I. Dagogo-Jack and A. T. Shaw, *Nat. Rev. Clin. Oncol.*, 2018, **15**, 81-94.
- X. Li, S. Lee and J. Yoon, *Chem. Soc. Rev.*, 2018, **47**, 1174-1188.
- S. Monro, K. L. Colon, H. M. Yin, J. Roque, P. Konda, S. Gujar, R. P. Thummel, L. Lilge, C. G. Cameron and S. A. McFarland, *Chem. Rev.*, 2019, **119**, 797-828.
- D. S. Wishart, *Nat. Rev. Drug Discov.*, 2016, **15**, 473-484.
- F. Kong, Z. Liang, D. Luan, X. Liu, K. Xu and B. Tang, *Anal. Chem.*, 2016, **88**, 6450-6456.
- L. Chen, L. Zhou, C. Wang, Y. Han, Y. Lu, J. Liu, X. Hu, T. Yao, Y. Lin, S. Liang, S. Shi and C. Dong, *Adv. Mater.*, 2019, **31**, 1904997.

This work reports a biopolymer-based micellar nanoplatform with redox-sensitivity for sequentially-enhanced mitochondria-targeted photodynamic therapy and hypoxia-amplified chemotherapy against CD44-positive tumors.

View Article Online
DOI: 10.1039/D0CC03667F

